PCCP

RSC Publishing

PAPER

View Article Online
View Journal | View Issue

The effect of axial ligand on the oxidation of syringyl alcohol by Co(salen) adducts†

Cite this: *Phys. Chem. Chem. Phys.*, 2013, **15**, 7328

Thomas Elder,*[a] Joseph J. Bozell[b] and Diana Cedeno[b]

Received 7th December 2012,
Accepted 2nd April 2013

DOI: 10.1039/c3cp44404j

www.rsc.org/pccp

Experimental work on the oxidation of the lignin model, syringyl alcohol, using oxygen and a Co(salen) catalyst has revealed variations in yield with different imidazole-based axial ligands. A reasonable linear relationship was found between product yield and pK_a of the axial ligand. The current work, using density functional calculations, examined geometric, electronic, and energetic parameters to determine if additional quantitative relationships can be identified and used in subsequent catalyst design. Good relationships with yield were identified with the geometry of the salen ligand and the charge on the ligand nitrogen coordinated to the cobalt.

1. Introduction

With the advent of the biorefinery has come increased interest in lignin as a renewable carbon source for biobased chemicals and fuels. Although lignin can account for up to 25% of the dry weight of lignocellulosic biomass, methods for the selective conversion of its complex and heterogeneous phenylpropanoid structure into discrete, low molecular weight aromatic compounds have remained elusive. This structural heterogeneity arises during lignin biosynthesis, which proceeds *via* conversion of three primary lignin monomers into highly delocalized phenoxy radicals, and subsequent coupling of these radicals at sites of high unpaired electron density. Furthermore, processes developed to isolate lignin from biomass[1] in various biorefinery scenarios can dramatically alter this native distribution of substructures.

Selective oxidations with molecular O_2 catalyzed by Co-Schiff base complexes can exploit these structural changes, affording processes potentially able to valorize lignin through the production of discrete, low molecular weight aromatic compounds. We have reported that O_2 converts *para*-substituted lignin model phenols to *para*-benzoquinones using Co-Schiff base catalysts.[2] Syringyl models were converted to 2,6-dimethoxybenzoquinone (DMBQ) in good to excellent yield. These reactions were suggested to proceed by the initial coordination of an axial ligand (L, typically pyridine) to a Co-Schiff base catalyst such as Co(salen) (Fig. 1, reaction I) followed by addition of O_2 to form a catalytically active Co-superoxo adduct (Fig. 1, reaction II).[3] The axial ligand is required for effective catalyst reactivity, as Co(salen) itself binds O_2 poorly.[4] Subsequently, the superoxo adduct abstracts a phenolic hydrogen from the substrate (Fig. 1, reaction III) resulting in a phenoxy radical, which combines with a second equivalent of the superoxo adduct (Fig. 1, reaction IV). The final step (Fig. 1, reaction V) results in the formation of the quinone oxidation product and formaldehyde. The critical step of the oxidation appears to be the ability of the Co-superoxo intermediate to remove a phenolic hydrogen from the substrate as affected by the presence or absence of the axial ligand. For example, the 5-coordinate complexes Co(salpr) and Co(N–Me salpr) converted syringyl alcohol to DMBQ, while syringaldehyde was more effectively oxidized with 4-coordinate Co(salen) in the absence of an axial ligand. Monomethoxylated phenols, which are less able to lose a phenolic hydrogen showed low reactivity. More recently, we reported that the yields of DMBQ from syringyl alcohol varied with a series of imidazole bases as the axial ligand[5] and that the yields were correlated to the pK_a of the conjugate acid of the ligand (R^2 = 0.92).

Due to the well-established O_2 carrying capability of Co-Schiff base complexes,[6] considerable computational and electronic structure research has probed the fundamentals of their behavior.[7–15] A range of computational intensity has been reported for Co-Schiff base compounds, including INDO,[7,13,14] *ab initio* Hartree–Fock[8] and the more recent density functional methods, such as the use of B3LYP results for axially substituted pyridine complexes and oxygenated adducts of Co(acacen) and Co(salen).[16,17] Upon geometry optimization the pyridine adducts of both Co(acacen) and Co(salen) adopted an ''umbrella''

[a] *USDA-Forest Service, Southern Research Station, 2500 Shreveport Highway, Pineville, LA 71360, USA. E-mail: telder@fs.fed.us; Fax: +1-318-473-7246; Tel: +1-318-473-7008*

[b] *Center for Renewable Carbon, and the Center for the Catalytic Conversion of Biomass (C3Bio), University of Tennessee, 2506 Jacob Drive, Knoxville, TN 37996-4570, USA. E-mail: jbozell@utk.edu; Fax: +1-865-946-1109; Tel: +1-865-974-5991*

† Electronic supplementary information (ESI) available. See DOI: 10.1039/c3cp44404j

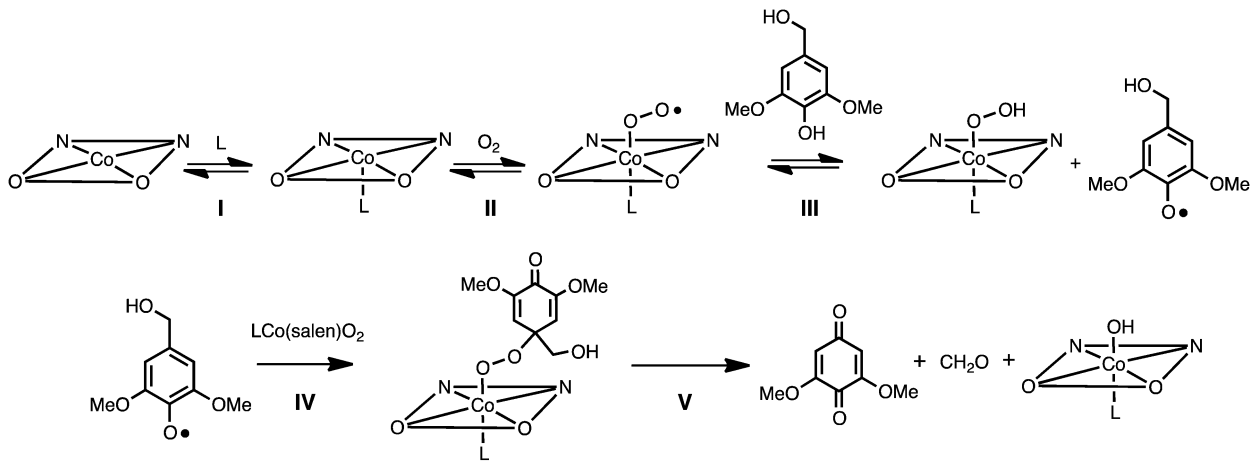

Fig. 1 Reactions of Co(salen).

conformation in which the salen ligand is distorted from planarity. It was also found that the bulk of the unpaired spin density of the Co(acacen) superoxo adduct was located on the axial oxygens. In work on the effect of the axial ligand,[8] changes in the enthalpy of oxygenation were related to the energy of the $3d_z^2$ orbital of the complex.

Based on these relationships and recent results, the current study was initiated to determine if the steric and electronic diversity of the imidazole ligands offered additional factors that affect the ability of the Co catalyst to remove the phenolic hydrogen from the substrate, and thus, affect the yield of quinone. Electronic and structural characteristics of a series of complexes of Co(salen) with axial imidazole ligands, and the corresponding superoxo adducts resulting from the reaction of the Co(salen)–imidazole complexes with O_2 have been evaluated. Reaction energetics of each step in the mechanism of Fig. 1 have been calculated to determine if quantitative relationships can be developed with the reaction yields, which could ultimately lead to *de novo* selection of axial ligands for specific purposes.

2. Results and discussion

The calculations for complexes of Co(salen) (**1**) with imidazoles **2–6** and their corresponding O_2 adducts were performed using the B3LYP density functional method. Paired calculations were done with the 6-31G(d) basis set for all atoms (designated as 6-31G(d)) and a mixed basis set using 6-31G(d) for C, H, O, and N, and LANL2DZ for the Co atom (designated as 6-31G(d)/LANL2DZ) (Optimized geometries can be found in the ESI†). While the different basis sets resulted in different absolute values for the various parameters that were evaluated, it will be seen that in general similar trends were found with each method.

To be consistent with the literature,[15] compounds **2a–6a** are referred to as complexes, while the superoxo compounds **2b–6b** are referred to as adducts. Fig. 2 summarizes the complexes examined, the Cartesian axes used for the calculations, and numbering of key atoms within the various structures.

For calibration purposes, the calculated orbital energies and assignments of **1** and imidazole adduct **2b** were compared to the literature (Fig. 3). The singly occupied orbital for **1** is the d_{yz}, which has been the topic of some debate in the literature, with some authors proposing the d_{yz} and others the d_z^2.[9] The d_{xy} is the highest energy orbital and unoccupied for **1**. Among the remaining occupied d-orbitals, there are some subtle variances in ordering that differ from reported results, but these are accounted for by the differences between the current density functional theory and the extended Hückel calculations found in the literature,[10,12] the use of truncated models of the salen ligand, or differences in the axial ligand.[8,15]

The unoccupied d_{xy} is also the highest energy in **2b**, and the unpaired electron is found to reside in the oxygen-p_y orbital, which is consistent with the literature.[11,15] All adducts resulted in similar ordering of atomic orbitals except for the 2,4-dimethylimidazole adduct **6b** in which there appears to be considerable mixing, while still retaining the oxygen-p_y as the singly occupied orbital. From these results it was concluded that the current methods are giving results that are comparable with the previous investigations.

2.1 Geometric results

For illustrative purposes, the optimized geometry for the 2,4-dimethylimidazole adduct **6b** is shown in Fig. 4a. The distortion of the salen ligand from planarity is the most striking of the geometric results, and is consistent with ''umbrella'' conformation previously reported[15] and observed by X-ray.[18,19] This ''book'' angle, formed by atoms 19-1-30 (Fig. 2b), was found to vary with the axial ligand for both the complexes **2a–6a** and adducts **2b–6b** (Fig. 4b), with the largest deviation resulting from 2,4-dimethylimidazole substitution. Using the all atom 6-31G(d) basis set, the structurally similar imidazole : 1-methylimidazole (**2b : 3b**) and 2-methyl : 1,2-dimethylimidazole (**4b : 5b**) adduct pairs do not experience significantly different steric interaction with the salen ligand, exhibiting book angles that are similar to each other, and consistent between the complexes and oxygenated adducts.

Complex	L1	L2
1, Co(salen)	none	none
2a	Imidazole	none
2b	Imidazole	O_2
3a	1-methylimidazole	none
3b	1-methylimidazole	O_2
4a	2-methylimidazole	none
4b	2-methylimidazole	O_2
5a	1,2-dimethylimidaozle	none
5b	1,2-dimethylimidaozle	O_2
6a	2,4-dimethylimidaozle	none
6b	2,4-dimethylimidaozle	O_2

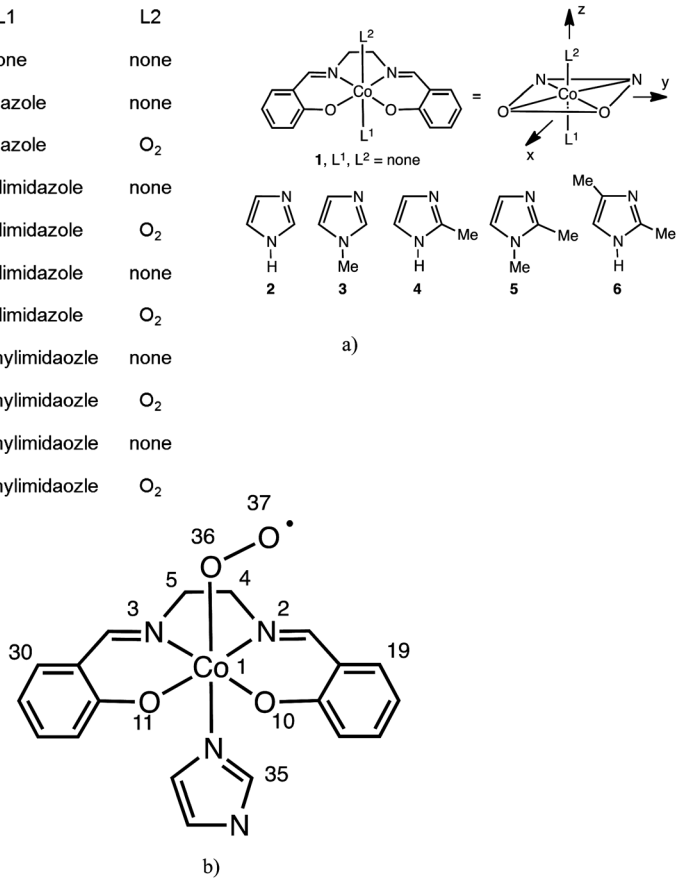

Fig. 2 (a) Structures examined in the current work, (b) key atom numbers for the Co(salen) structures.

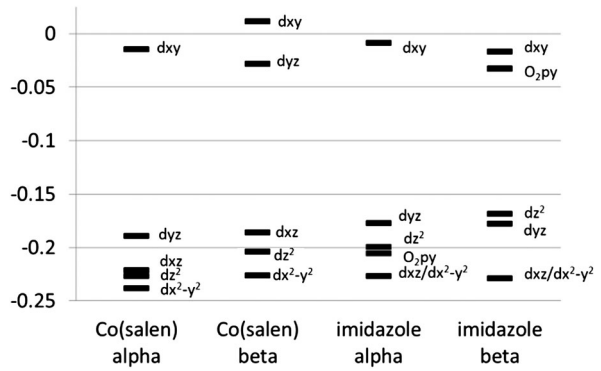

Fig. 3 Orbital energies (a.u.) and ordering for Co(salen) and the imidazole adduct.

In contrast, the 2-methylimidazole complex **4a** exhibits a salen ligand that is markedly flatter than its corresponding adduct **4b** as a result of its ligand being rotated away from the *y*-axis of the salen ligand by about 80° when using 6-31G(d). Similarly, a rotation of 112° was found for the 1-methylimidazole complex **3a**. Experimental evidence[18,20] indicates that in general, the axial ligand is oriented parallel to the *y*-axis, and as a consequence all optimizations were initiated in this conformation. The rotation to a more perpendicular conformation undoubtedly accounts for the relative flatness of **4a** in which the steric interaction between the substituent and the salen has been markedly reduced by placing the 2-methyl substituent in the gap between the oxygens of the salen ligand. Repeating the calculation on **4a** but constraining the 2-methylimidazole ligand to a parallel conformation resulted in a salen book angle consistent with its corresponding adduct **4b**. The contrasting lack of deviation in book angles for the 1-methylimidazole complex **3a** and its adduct **3b** is rationalized by the relative remoteness of the methyl substituent to the salen which affords reduced steric interaction.

Nonetheless, a steric argument does not explain why the 1-methylimidazole ligand, which would be expected to have much lower steric requirements, rotates at all, nor does it explain why the orientation of the more sterically hindered 1,2-dimethylimidazole ligand is parallel to the salen *y*-axis in **5a**. More fundamentally it is proposed that these conformational observations result from additional incorporation of a weak π bonding interaction between the HOMO of the complex (d_{yz}) and an appropriate π* orbital on the ligand. The HOMO of the complex is strongly d_{yz}, which accounts for the orientation of the 1-methylimidazole ligand, but the difference in energy between the observed rotated conformation and the parallel orientation for **3a** is only 1.48 kcal, highlighting that any such stabilization is small because of the weak π acceptor ability of imidazoles.[21] The weakness of this bonding is further

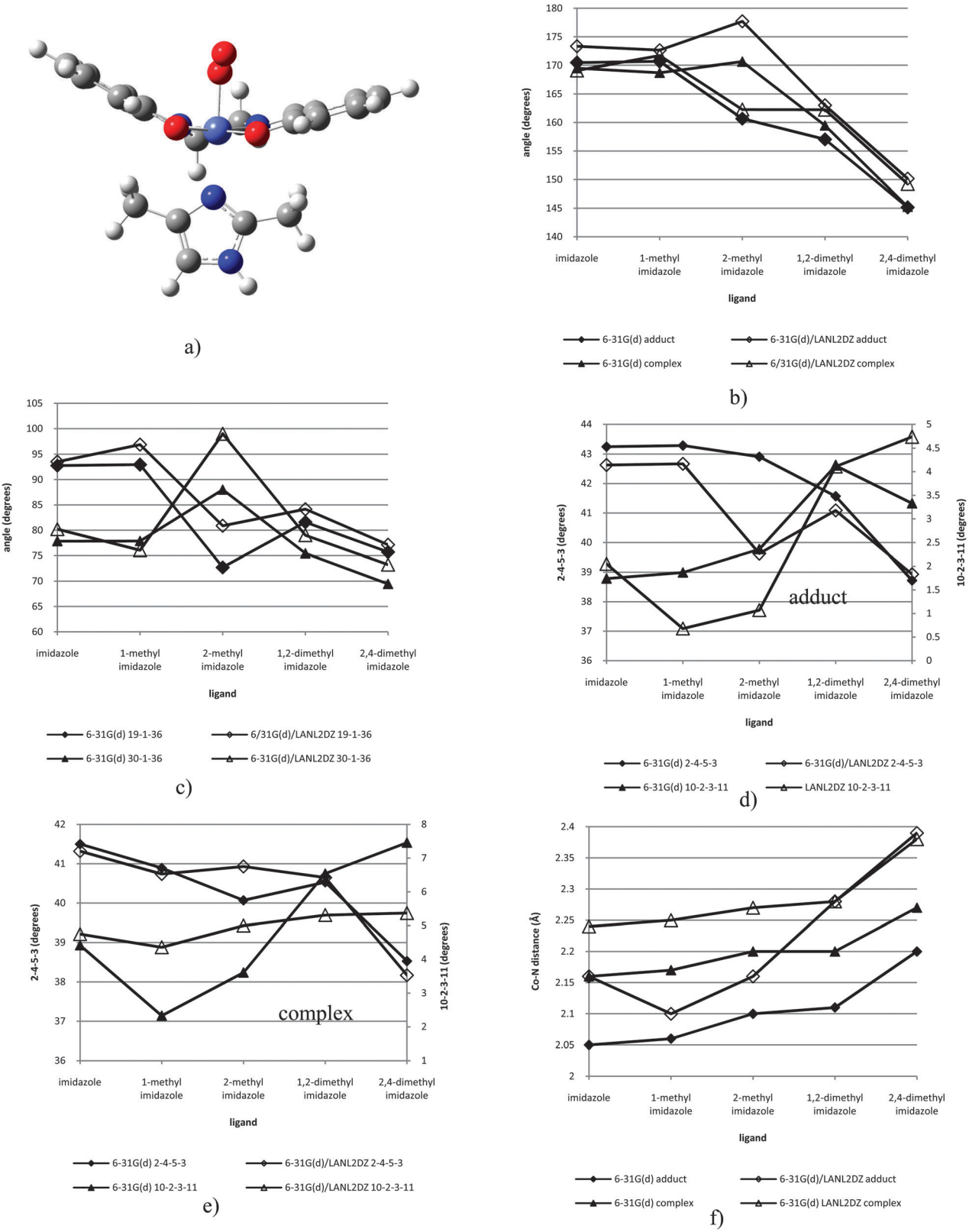

Fig. 4 Geometric results.

illustrated in the return of the 1,2-dimethylimidazole complex **5a** to a parallel conformation. This behavior is attributed to the increased electron density of the ligand induced by the presence of a second methyl group, reducing its ability to act

as a π-acceptor ligand. Further, although the d_{xz} orbital could participate in similar π bonding, the orbital coefficients for the d_{xz} orbital in the 1- and 2-methylimidazole complexes suggest that it has a preferentially stronger interaction at lower energies (HOMO-3 and HOMO-5) with the $d_{x^2-y^2}$ orbital and may not be at appropriate energy for effective overlap with the π* network of the unsubstituted imidazole ligand. In addition, the paired calculation using the 6-31G(d)/LANL2DZ mixed basis set orients the 2-methylimidazole ligand in **4a** parallel to the *y*-axis, but rotates the ligand in adduct **4b** to about 80°, highlighting the low energy barrier between these conformations.

The presence of π-bonding, even if it is relatively weak, is reported to affect the geometry of metal complexes. π-Bonding strongly influences whether transition metal dithiolate complexes adopt an octahedral or prismatic structure.[22] π-Backbonding was also used to explain the geometry of a series of Co dioximato complexes.[23] Similar π-bonding effects have been reported to influence the geometry of other metal–imidazole complexes. The complex $[Fe(TMP)(5\text{-MeHIm})_2]ClO_4$ crystallizes in two forms, one with the planes of the imidazole ligands parallel to each other, and the other with the planes perpendicular.[24] This mixed orientation is explained as a balance between crystal field stabilization through π-bonding in the parallel case, and minimization of steric effects that favor the perpendicular orientation. However, the stabilization energy resulting from either orientation is calculated as less than 3 kcal mol^{-1}, similar to the stabilization energy calculated for the Co(salen) complexes. Imidazole ligands are known to serve as π-donors, but it is proposed that weak π-acceptor behavior is most consistent with the relatively low oxidation state of the Co,[25] the orientation of 1,2-dimethylimidazole as a weaker acceptor, and the parallel orientation of all imidazole ligands observed for the adducts **2b–6b**.

A comparison of the angles between atoms 19-1-36 and atoms 30-1-36 shows that the book angle of the adducts is not distributed symmetrically (Fig. 4c), resulting in a half-chair conformation of the ethylene bridge as evidenced by a dihedral angle (atoms 2-4-5-3) of ~37–43° for all adducts (Fig. 4d), which is consistent with the values of ~45° reported by Henson *et al.*[15] This dihedral angle is somewhat lower for the complexes (Fig. 4e) than the adducts, while for both, the largest angle is exhibited with imidazole as the axial ligand, and the smallest by the 2,4-dimethylimidazole as the axial ligand. The dihedral angle formed by atoms 10-2-3-11 (Fig. 4d and e), indicative of the planarity of the salen ligand about the Co atom is reasonably small, but with some degree of variability. The complexes (Fig. 4e) are slightly more planar than the adducts (Fig. 4d), while the dihedral angle generally increases with increasing methyl substitution on the axial ligand, especially at the 2-position. The 6-31G(d)/LANL2DZ calculations give values for the 10-2-3-11 angle that are within 1.5° of the 6-31G(d) calculations. The Co–N(ligand) distance ranges from *ca.* 2.05–2.27 Å, with the distances being greater for the adducts (Fig. 4f), and with the use of the mixed 6-31G(d)/LANL2DZ basis set, albeit with similar trends, in which this distance increases with methyl substitution.

2.2 Electronic results

Natural Bond Order charges and spin densities are shown in Fig. 5 and 6, respectively. The Co atom exhibits a range of charges from 0.95–1.01, the highest of which is associated 2,4-dimethylimidazole (Fig. 5a). The results for the complexes and adducts parallel each other, with the complexes exhibiting a higher positive charge. Similarly, the axial ligand nitrogen charges are largely parallel between the adducts and complexes, varying from −0.54 to −0.46, (Fig. 5b) with the largest negative charge again present on the 2,4-dimethylimidazole adduct. The nitrogen charge exhibits a generally inverse relationship with the Co charge. These patterns are similar to those observed for the 19-1-30 angle and the distance between the Co and ligand nitrogen. The 6-31G(d) calculations show that the charges on the O(36) are consistently more negative than O(37) (Fig. 5c), but both exhibit similar trends which are in accord with the Co charge, with the negative charge decreasing with methyl substitution. These values for the mixed 6-31G(d)/LANL2DZ calculations are more variable, but are internally consistent and parallel. Spin densities for the Co adduct (Fig. 6a) are exclusively negative, meaning an excess of beta electron density is present at this position. Within the complexes (Fig. 6b), the Co spin densities are positive and inversely related to the adducts. Both of the oxygens in the adducts (Figs. 6c and d) have an excess of alpha electrons, and are the sites of largest unpaired electron density. The axial ligand nitrogen has negligible spin density. These observations agree with the spin density plots, as illustrated by the imidazole adduct **2b** (Fig. 6e). It is interesting to note that the alpha spin density centered on the oxygens resembles a p-orbital, while the beta density on the Co has the appearance of a d_z^2 atomic orbital. The spin density plot of the imidazole complex **2a** (Fig. 6f) is also consistent with the results in Fig. 5c, in which an excess of alpha electrons is found to be present on the Co, in a plot resembling a d_z^2 atomic orbital.

Based on these observations indicating some degree of similarity in trends between electronic and geometric results, and in order to make a more comprehensive comparison, linear R^2 values are shown in Tables 1 and 2. Generally strong linear relationships with charge and spin density can be seen for the 19-1-30 book angle of the Co-salen ligand and the Co–N (ligand) distance for both the complexes and adducts with both basis sets. Interestingly, the 6-31G(d) basis set results show strong correlations within the 2-4-5-3 dihedral and but weaker relationships for the 10-2-3-11 dihedral angle, while this trend is reversed by the application of the mixed 6-31G(d)/LANL2DZ basis set. Otherwise there were no major differences observed between the computational methods. It is apparent from these data that the geometric and electronic parameters are interrelated, but it is not clear which factor is in primary control, whether changes in structure induce changes in the electronics, or *vice versa*.

It is interesting, and surprising to note that the complexes and adducts with the highest positive charge at Co also bear the most strongly donating axial imidazole ligands. Electrochemical studies of a series of $Co–O_2$ carriers show that systems whose

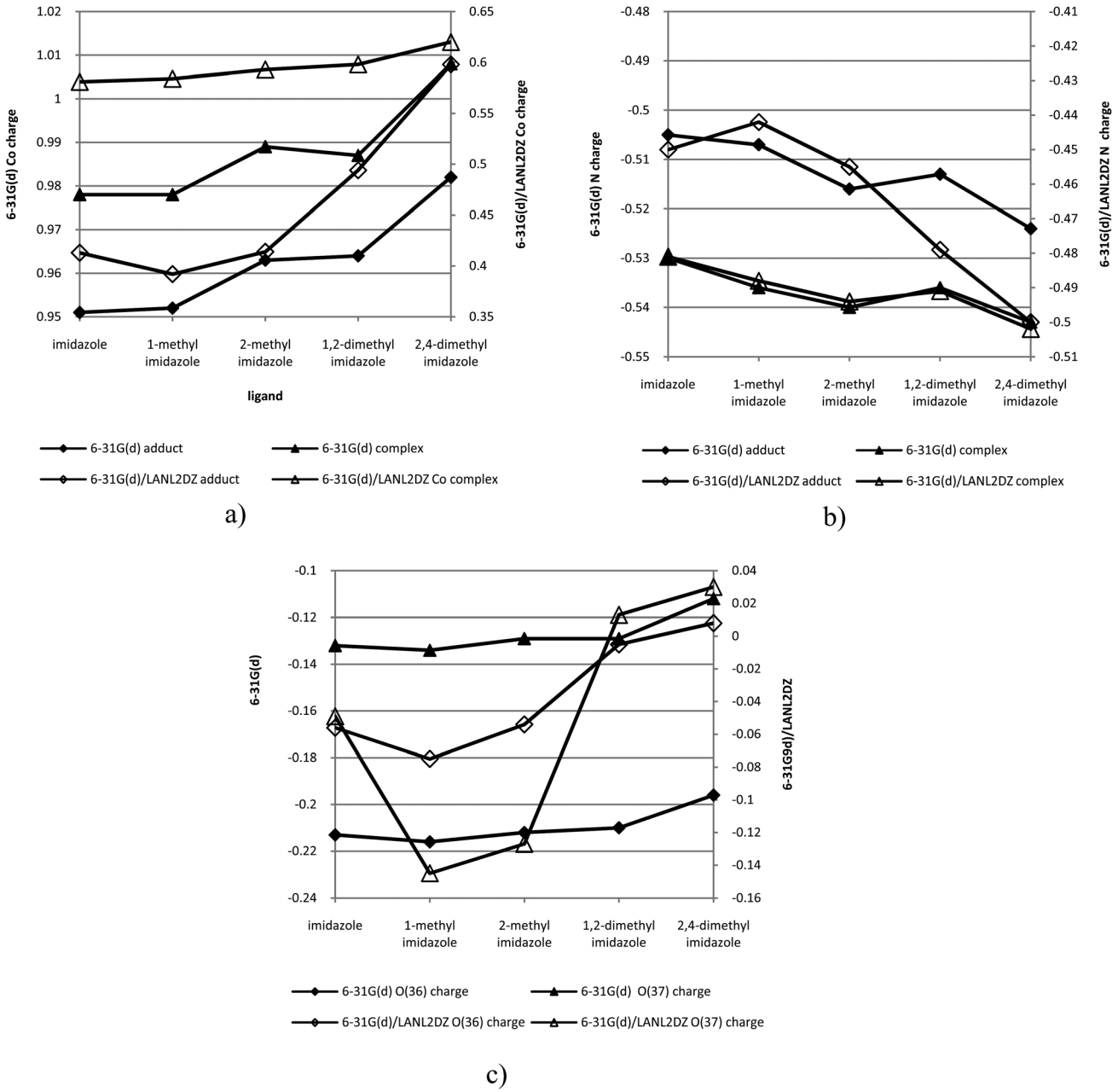

Fig. 5 NBO charge results.

planar ligands have higher electronegativity also bind O_2 more poorly because there is less electron density at the Co center.[26] In the current work the effect of electronegativity of the planar salen ligand on Co charge should be negligible as the calculated bond lengths between the Co and the salen heteroatoms in all complexes are within 0.02 Å of one another. In contrast, the distortion of the salen ligand resulting from the coordination of sterically hindered imidazole ligands would have a significant effect on the Co charge. As the distortion of the salen ligand increases, interaction of the Co with the donor nitrogen and oxygen atoms of the salen ligand is decreased, effectively increasing the positive charge at Co. It is suggested that the computational analysis reveals the presence of counterbalancing effects on the reactivity of Co(salen)–imidazole complexes and their adducts with O_2. Strongly donating ligands promote binding of Co(salen) complexes to O_2 by raising the energy of the Co d_z^2 orbital, promoting transfer of an electron to the O_2.[11] Attempts to use sterically hindered donors to achieve that improved binding, however, counterbalances the donor ability of the imidazole ligand by distorting the salen and reducing the effect of the donor that might otherwise be expected. The result is that ligands showing higher donor ability do not have a significantly better effect on yield than poorer donors.

2.3 Energetics

The energetics for each of the reaction steps in Fig. 1, with the exception of reaction II, show similar trends using either the

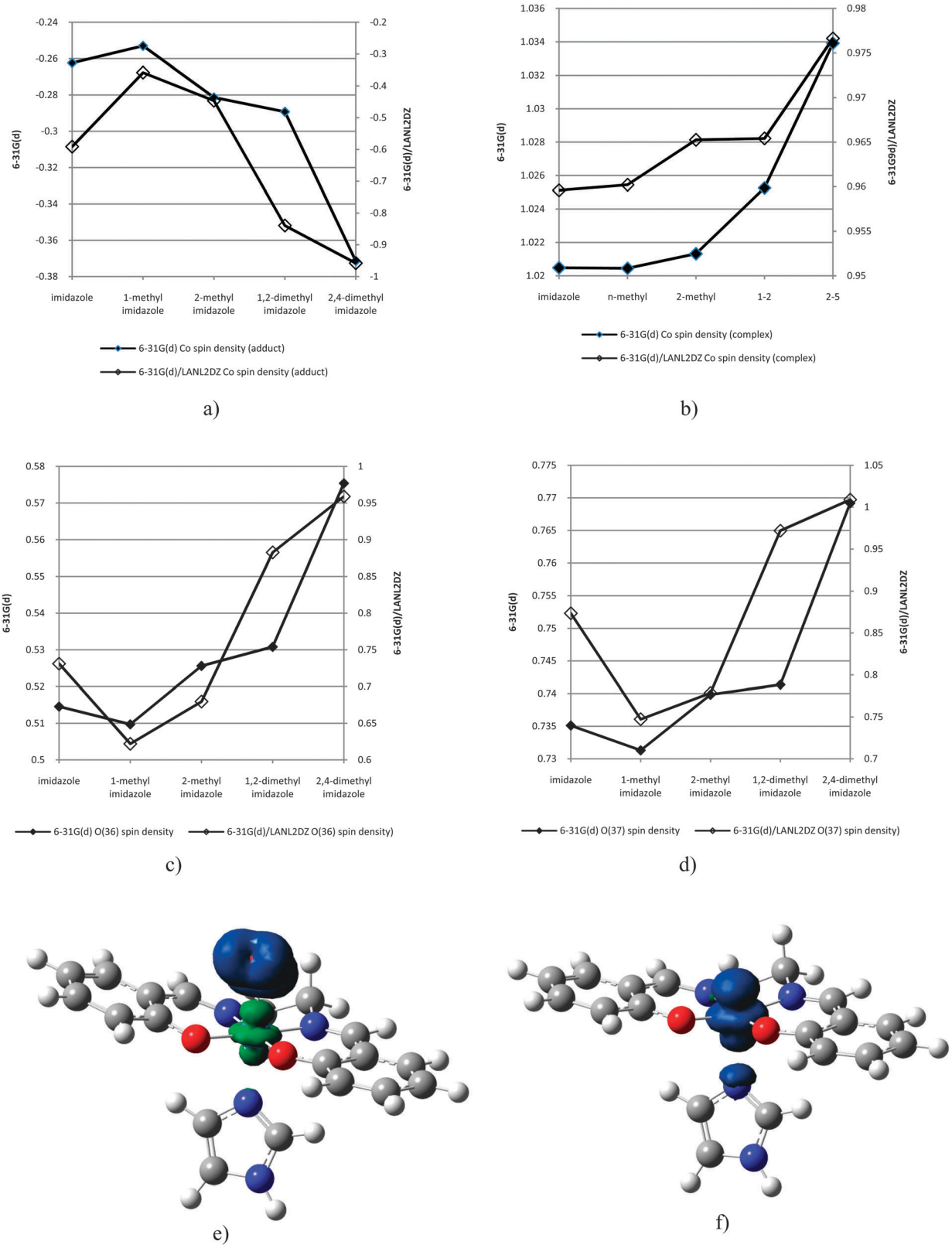

Fig. 6 NBO spin density results.

6-31G(d) or 6-31G(d)/LANL2DZ basis sets (data shown in ESI†). The energy associated with the coordination of the ligands to Co(salen) (reaction I) is closely related to the book angle of the complex for both basis sets with R^2 values in excess of 0.9

Table 1 *R*-square values for adducts and complexes (in parentheses) 6-31G(d)

	19-1-30 angle	19-1-36 angle	30-1-36 angle	2-4-5-3 dihedral angle	10-2-3-11 dihedral angle	Co–N(ligand) distance
Co charge	0.98(0.78)	0.60(N/A)	0.24(N/A)	0.91(0.96)	0.44(0.58)	0.99(0.99)
O(36) charge	0.86(N/A)	0.33(N/A)	0.44(N/A)	0.96(N/A)	0.30(N/A)	0.92(N/A)
O(37) charge	0.86(N/A)	0.38(N/A)	0.36(N/A)	0.93(N/A)	0.25(N/A)	0.94(N/A)
N(ligand) charge	0.92(0.44)	0.76(N/A)	0.09(N/A)	0.76(0.87)	0.36(0.15)	0.93(0.75)
Co spin density	0.91(0.97)	0.42(N/A)	0.37(N/A)	0.96(0.80)	0.33(0.75)	0.96(0.91)
O(36) spin density	0.92(N/A)	0.42(N/A)	0.36(N/A)	0.96(N/A)	0.35(N/A)	0.97(N/A)
O(37) spin density	0.88(N/A)	0.38(N/A)	0.38(N/A)	0.95(N/A)	0.28(N/A)	0.94(N/A)
N(ligand) spin density	0.02(0.93)	0.33(N/A)	0.31(N/A)	0.01(0.89)	0.17(0.63)	0.00(0.96)
Energy of reaction I	0.83(0.92)	0.27(N/A)	0.53(N/A)	0.95(0.69)	0.38(0.83)	0.86(0.83)
Energy of reaction II	0.92(0.69)	0.67(N/A)	0.14(N/A)	0.80(0.98)	0.37(0.46)	0.96(0.97)
Energy of reaction III	0.68(0.81)	0.15(N/A)	0.59(N/A)	0.74(0.38)	0.82(0.87)	0.61(0.54)
Energy of reaction IV	0.88(0.55)	0.80(N/A)	0.05(N/A	0.69(0.90)	0.29(0.46)	0.87(0.89)
Energy of reaction V	0.47(0.11)	0.93(N/A)	0.07(N/A)	0.22(0.57)	0.09(0.11)	0.44(0.48)
Total energy	0.90(0.97)	0.31(N/A)	0.54(N/A)	0.99(0.82)	0.51(0.52)	0.92(0.88)

representing adoption of sterically favorable orientations and the availability of weak π-bonding interactions.

Subsequent coordination of O_2 (reaction II) is also strongly correlated with the book angle of the adduct (R^2 = 0.92) for the 6-31G(d) calculation. In both reactions I and II the exothermicity of the reaction generally decreases with methyl substitution on the axial ligand, with coordination of the bulky 2,4-dimethylimidazole being least exothermic. Calculations using the 6-31G(d)/LANL2DZ basis set exhibits somewhat more sensitivity to the electronic nature of the ligand for complexes **2b** and **3b** in that the stronger donor (1-methylimidazole) affords a more exothermic reaction than observed using the 6-31G(d) basis set.

The energy calculated for the 2-methyl complex **4a** in reaction II is somewhat out of line for calculations using either 6-31G(d) or 6-31G(d)/LANL2DZ, and likely reflects the different starting conformations of the respective Co(salen)–imidazole complex. Complex **4a** as results from the 6-31G(d) minimization begins with its 2-methylimidazole ligand oriented nearly perpendicular to the *y*-axis of the salen ligand. As the oxygen binds, the ligand is rotated nearly parallel to the *y*-axis, increasing the steric hindrance with the bound oxygen, and affording a less exothermic reaction than predicted. In contrast, the conformation of **4a** from the 6-31G(d)/LANL2DZ minimization begins with the ligand nearly parallel to the *y*-axis, and rotates it almost perpendicular upon binding of O_2. The result is a more exothermic reaction than predicted.

Conversion of syringyl alcohol into the corresponding phenoxy radical upon reaction with the Co-superoxo complexes (reaction III) generally continues this trend, and although differing in absolute values the different basis sets largely parallel each other. Imidazole, 1-methylimidazole and 2-methylimidazole adducts **2b–4b** exhibit approximately equal energies of reaction, with the better donors as indicated by pK_a affording slightly more endothermic reactions. The most sterically hindered ligand, 2,4-dimethylimidazole, gives the most endothermic reaction which is likely a reflection of the severe book angle of the complex that hinders approach of syringyl alcohol. In contrast, the energy value calculated for the 1,2-dimethylimidazole adduct **5b** appears unusually large. The book angle of this adduct is almost the same as the 2-methylimidazole adduct **4b** (157.02° and 157.62°, respectively) and the improved donor ability of the complex would suggest a more exothermic reaction. The reason for this observation remains unclear.

Coupling of the phenoxy radical with the superoxo complex (reaction IV) again shows largely steric control, with the most exothermic reactions observed for the least sterically demanding ligands. The improved donor ability of 1,2-dimethylimidazole affording an adduct with higher spin density at the bound terminal oxygen results in a slightly more exothermic reaction with the phenoxy radical than observed with the 2-methylimidazole adduct, which would have otherwise similar steric requirements.

The final step in the process, expulsion of the DMBQ product (reaction V), also appears to be driven by sterics. The most sterically hindered coupling product, derived from the 2,4-dimethylimidazole adduct, affords the most exothermic reaction, as would be expected by release of the product. The smaller ligands show correspondingly less exothermic reactions as the steric release would be expected to be lower. The intermediate complex formed from 1,2-dimethylimidazole is interesting, as it is slightly less exothermic than might be expected, but may be the result of stronger bonding to the phenoxy radical in the preceding step.

Close relationships are also found between reaction I and the total energy (R^2 > 0.94) indicating that changes in the energetics associated with reaction I would be reflected in the overall energy of reaction for the oxidation of the substrate. Perhaps more interestingly, a strong correlation is detected between the overall energy of the reactions and the spin density of the Co in the ligated complexes (Tables 1 and 2). From this relationship it would appear that the Co spin density is differentially stabilizing the complexes, ultimately accounting for analogous changes in the total reaction energy.

2.4 Correlations with experimental yield data

Correlating calculated and experimental properties provides insight regarding the mechanism responsible for transforming phenols to benzoquinones. Understanding these relationships could be used to predict catalytic activity prior to costly and time-consuming synthetic and analytical work. To this end,

Table 2 *R*-square values for adducts and complexes (in parentheses) 6-31G(d)/LANL2DZ

	19-1-30 angle	19-1-36 angle	30-1-36 angle	2-4-5-3 dihedral angle	10-2-3-11 dihedral angle	Co–N(ligand) distance
Co charge	0.94(0.95)	0.56(N/A)	0.21(N/A)	0.50(0.88)	0.86(0.64)	0.98(0.97)
O(36) charge	0.78(N/A)	0.60(N/A)	0.13(N/A)	0.44(N/A)	0.96(N/A)	0.96(N/A)
O(37) charge	0.71(N/A)	0.29(N/A)	0.26(N/A)	0.15(N/A)	0.96(N/A)	0.81(N/A)
N(ligand) charge	0.87(0.80)	0.66(N/A)	0.13(N/A)	0.55(0.73)	0.89(0.44)	0.99(0.81)
Co spin density	0.81(0.97)	0.43(N/A)	0.23(N/A)	0.28(0.89)	0.99(0.61)	0.93(0.98)
O(36) spin density	0.84(N/A)	0.49(N/A)	0.20(N/A)	0.35(N/A)	0.99(N/A)	0.96(N/A)
O(37) spin density	0.76(N/A)	0.35(N/A)	0.25(N/A)	0.20(N/A)	0.98(N/A)	0.87(N/A)
N(ligand) spin density	0.37(0.94)	0.18(N/A)	0.12(N/A)	0.05(0.93)	0.76(0.53)	0.53(0.99)
Energy of reaction I	0.69(0.99)	0.78(N/A)	0.03(N/A)	0.78(0.82)	0.60(0.68)	0.85(0.94)
Energy of reaction II	0.53(0.22)	0.08(N/A)	0.38(N/A)	0.01(0.17)	0.80(0.42)	0.56(0.21)
Energy of reaction III	0.91(0.75)	0.46(N/A)	0.26(N/A)	0.35(0.67)	0.95(0.70)	0.97(0.75)
Energy of reaction IV	0.28(0.84)	0.95(N/A)	0.07(N/A	0.99(0.48)	0.27(0.63)	0.52(0.65)
Energy of reaction V	0.05(0.13)	0.44(N/A)	0.77(N/A)	0.47(0.00)	0.01(0.16)	0.00(0.02)
Total energy	0.89(0.88)	0.59(N/A)	0.17(N/A)	0.51(0.78)	0.87(0.72)	0.98(0.88)

Table 3 shows relationships between yields and ligand pK_a for geometric/electronic and energetic results.

A high degree of correlation has been established between quinone yield and pK_a, as demonstrated by the R^2 value of 0.92. In general, the calculated values give a poorer fit to the yield data, with the strongest relationships exhibited by the 6-31G(d) calculations for adduct book angle, the 19-1-36 angle and the charge on the ligand nitrogen. In general, these fits were poorer with the 6-31G(d)/LANL2DZ basis set. For the most part, the R^2 values from the adducts are higher than those for complexes. It is interesting to note that the calculated parameters are much more closely related to pK_a with values of 0.90 and above for the book angle, ligand nitrogen charge of the adducts and the energy of reaction II (Table 3).

These data suggest that a correlation of computational results with observed experimental yields may result from combinatorial interactions between two or more factors. This interpretation may be supported by the multi-step nature of the overall oxidation reaction. Additional data points would be beneficial in terms of providing more coverage of the experimental space and allowing for the inclusion of additional terms into a multiple regression equation. Such evaluation is currently underway.

Table 3 *R*-square values with yield and pK_a

	6-31G(d)		6-31G(d)/LANL2DZ	
	Yield	pK_a	Yield	pK_a
19-1-30 angle	0.73(0.47)	0.91(0.63)	0.41(0.57)	0.53(0.81)
19-1-36 angle	0.60(N/A)	0.71(N/A)	0.65(N/A)	0.82(N/A)
30-1-36 angle	0.07(N/A)	0.11(N/A)	0.00(N/A)	0.00(N/A)
2-4-5-3 dihedral angle	0.51(0.57)	0.71(0.82)	0.59(0.38)	0.80(0.60)
10-2-3-11 dihedral angle	0.79(0.44)	0.64(0.52)	0.43(0.62)	0.49(0.69)
Co–N(ligand) distance	0.63(0.60)	0.86(0.85)	0.54(0.49)	0.69(0.74)
Co charge	0.65(0.55)	0.88(0.81)	0.52(0.65)	0.69(0.86)
O(36) charge	0.38(N/A)	0.62(N/A)	0.62(N/A)	0.68(N/A)
O(37) charge	0.38(N/A)	0.64(N/A)	0.26(N/A)	0.31(N/A)
N(ligand) charge	0.67(0.62)	0.90(0.78)	0.62(0.71)	0.76(0.90)
Co spin density	0.46(0.49)	0.71(0.69)	0.40(0.58)	0.48(0.82)
O(36) spin density	0.48(N/A)	0.72(N/A)	0.47(N/A)	0.55(N/A)
O(37) spin density	0.40(N/A)	0.66(N/A)	0.31(N/A)	0.37(N/A)
N(ligand) spin density	0.34(0.50)	0.17(0.73)	0.15(0.53)	0.14(0.78)
Energy of reaction I	0.37	0.58	0.48	0.74
Energy of reaction II	0.68	0.90	0.08	0.09
Energy of reaction III	0.59	0.58	0.39	0.53
Energy of reaction IV	0.55	0.80	0.52	0.75
Energy of reaction	0.36	0.53	0.11	0.15
Total energy	0.53	0.71	0.45	0.64

3. Methods

The structures examined are Co(salen) **1**, complexes **2a–6a** and their corresponding superoxo adducts **2b–6b** (Fig. 2a), with key atom numbers shown in Fig. 2b. The axial ligands under consideration are imidazole, 1-methylimidazole, 2-methylimidazole, 1,2-dimethylimidazole and 2,4-dimethylimidazole. All calculations were performed at the B3LYP level of theory using the 6-31G(d) basis set and a mixed basis set using 6-31G(d) for C, H, N, and O and the LANL2DZ basis set for Co. Full geometry optimization and frequency calculations were carried out to verify the identification of an energetic minimum. The use of mixed basis sets[15] and methods treating all atoms at the 6-31G(d) level have literature precedent[17,27] Furthermore, in a study on related ligated metal species, Takatani and co-workers[28] found that results from the B3LYP level of theory did not differ statistically from the more recent M0 functionals. The structures were modeled as neutral doublets (*i.e.* a single unpaired electron) with unrestricted calculations done for each structure. Natural Bond Order (NBO) charge and spin densities were determined, and the energetic values are zero point corrected. All calculations were done using Gaussian 09, revision B.01.[29] All calculations were done using the facilities of the Alabama Supercomputer Center in Huntsville, Alabama. The assistance of Dr David C. Young is gratefully acknowledged in this regard.

4. Conclusions

Computational results on the Co(salen) catalyzed oxidation of phenols to benzoquinones suggest that the reactivity of the process is influenced strongly by steric interactions around the Co center. Both calculated electronic features of the intermediate complexes and the energetics of the individual mechanistic steps are seen to change in a predictable manner as the size of the axial imidazole ligand changes. Where steric features are generally equivalent (for example, between complexes of 2-methylimidazole and 1,2-dimethylimidazole), electronic factors related to the donor

ability of the imidazole ligand can influence the reaction. The semi-quantitative nature of these results, notwithstanding, it is positive that some general trends can be seen in the geometric and electronic structure of the catalyst that could be exploited in developing the next generation of catalysts for lignin oxidation.

Notes and references

1 N. Mosier, C. Wyman, B. Dale, R. Elander, Y. Y. Lee, M. Holtzapple and M. Ladisch, *Bioresour. Technol.*, 2005, **96**, 673–686.
2 J. J. Bozell, B. R. Hames and D. R. Dimmel, *J. Org. Chem.*, 1995, **60**, 2398–2404.
3 A. Zombeck, R. S. Drago, B. B. Corden and J. H. Gaul, *J. Am. Chem. Soc.*, 1981, **103**, 7580–7585.
4 B. Rajagopalan, H. Cai, D. H. Busch and B. Subramaniam, *Catal. Lett.*, 2008, **123**, 46–50.
5 D. Cedeno and J. J. Bozell, *Tetrahedron Lett.*, 2012, **53**, 2380–2383.
6 D. Chen, A. E. Martell and Y. Z. Sun, *Inorg. Chem.*, 1989, **28**, 2647–2652.
7 P. Fantucci and V. Valenti, *J. Am. Chem. Soc.*, 1976, **98**, 3832–3838.
8 A. Dedieu, M. M. Rohmer and A. Veillard, *J. Am. Chem. Soc.*, 1976, **98**, 5789–5800.
9 M. A. Hitchman, *Inorg. Chem.*, 1977, **16**, 1985–1993.
10 C. Daul, C. W. Schläpfer and A. von Zelewsky, *Struct. Bonding*, 1979, **36**, 129–171.
11 R. S. Drago and B. B. Corden, *Acc. Chem. Res.*, 1980, **13**, 353–360.
12 C. Daul and J. Weber, *Helv. Chim. Acta*, 1982, **65**, 2486–2497.
13 M. Valko, R. Klement, P. Pelikan, R. Boca, L. Dlhan, A. Bottcher, H. Elias and L. Muller, *J. Phys. Chem.*, 1995, **99**, 137–143.
14 R. Boca, H. Elias, W. Haase, M. Huber, R. Klement, L. Muller, H. Paulus, I. Svoboda and M. Valko, *Inorg. Chim. Acta*, 1998, **278**, 127–135.
15 N. J. Henson, P. J. Hay and A. Redondo, *Inorg. Chem.*, 1999, **38**, 1618–1626.
16 M. Atanasov, E. J. Baerends, P. Baettig, R. Bruyndonckx, C. Daul, C. Rauzy and M. Zbiri, *Chem. Phys. Lett.*, 2004, **399**, 433–439.
17 R. I. Makhmutova, I. V. Vakulin, R. F. Talipov, E. M. Movsumade and D. A. Chuvashov, *J. Mol. Struct.*, 2007, **819**, 21–25.
18 M. Calligaris, D. Minichelli, G. Nardin and L. Randaccio, *J. Chem. Soc. A*, 1970, 2411–2415.
19 B. J. Kennedy, G. D. Fallon, B. Gatehouse and K. S. Murray, *Inorg. Chem.*, 1984, **23**, 580–588.
20 A. Avdeef and W. P. Schaefer, *J. Am. Chem. Soc.*, 1976, **98**, 5153–5159.
21 E. V. Dose and L. J. Wilson, *Inorg. Chem.*, 1978, **17**, 2660–2666.
22 J. L. Martin and J. Takats, *Can. J. Chem.*, 1989, **67**, 1914–1923.
23 S. A. Kubow, K. J. Takeuchi, J. J. Grzybowski, A. J. Jircitano and V. L. Goedken, *Inorg. Chim. Acta*, 1996, **241**, 21–30.
24 O. Q. Munro, J. A. Serth-Guzzo, I. Turowska-Tyrk, K. Mohanrao, T. K. Shokhireva, F. A. Walker, P. G. Debrunner and W. R. Scheidt, *J. Am. Chem. Soc.*, 1999, **121**, 11144–11155.
25 C. R. Johnson, C. M. Jones, S. A. Asher and J. E. Abola, *Inorg. Chem.*, 1991, **30**, 2120–2129.
26 M. J. Carter, D. P. Rillema and F. Basolo, *J. Am. Chem. Soc.*, 1974, **96**, 392–400.
27 G. V. Girichev, N. I. Giricheva, N. V. Tverdova, A. O. Simakov, N. P. Kuz'mina and O. V. Kotova, *J. Struct. Chem.*, 2010, **51**, 223–230.
28 T. Takatani, J. S. Sears and C. D. Sherrill, *J. Phys. Chem. A*, 2010, **114**, 11714–11718.
29 M. J. Frisch, G. W. Trucks, H. B. Schlegel, G. E. Scuseria, M. A. Robb, J. R. Cheeseman, G. Scalmani, V. Barone, B. Mennucci, G. A. Petersson, H. Nakatsuji, M. Caricato, X. Li, H. P. Hratchian, A. F. Izmaylov, J. Bloino, G. Zheng, J. L. Sonnenberg, M. Hada, M. Ehara, K. Toyota, R. Fukuda, J. Hasegawa, M. Ishida, T. Nakajima, Y. Honda, O. Kitao, H. Nakai, T. Vreven, J. Montgomery, J. E. Peralta, F. Ogliaro, M. Bearpark, J. J. Heyd, E. Brothers, K. N. Kudin, V. N. Staroverov, R. Kobayashi, J. Normand, K. Raghavachari, A. Rendell, J. C. Burant, S. S. Iyengar, J. Tomasi, M. Cossi, N. Rega, J. M. Millam, M. Klene, J. E. Knox, J. B. Cross, V. Bakken, C. Adamo, J. Jaramillo, R. Gomperts, R. E. Stratmann, O. Yazyev, A. J. Austin, R. Cammi, C. Pomelli, J. W. Ochterski, R. L. Martin, K. Morokuma, V. G. Zakrzewski, G. A. Voth, P. Salvador, J. J. Dannenberg, S. Dapprich, A. D. Daniels, O. Farkas, J. B. Foresman, J. V. Ortiz, J. Cioslowski and D. J. Fox, *Gaussian 09; Revision B.01*, Gaussian, Inc., Wallingford, CT, 2009.